Robust and self-adaptable 5-finger 4-DoA robotic hand

André Farinha
andre.farinha@ist.utl.pt

Instituto Superior Técnico, Lisboa, Portugal

April 2015

Abstract

In this thesis a hand is developed that is robust, compliant and conformable, as the existing simpler hands, by using underactuation and serial elastic actuation but that is also dexterous, as existing complex systems, through a kinematics design based on the abstraction of the human hand functionalities. The developed hand is accessible, human-sized, almost self-contained, has a mass of 0,57kg and a maximum payload of 4.5kg, specifications which are among the most advanced in similar systems, enabling it to be easily adapted into existing arms without greatly affecting their payload. The hand accomplishes 41 of the 49 grasps in Feix and Cutkosky taxonomies. A magnetoresistive tactile sensor is developed that presents a non-linear response curve, a resolution under $(2.513 \pm 0.040) \times 10^4$ Pa and a force sensing range greater than $(7.123 \pm 0.016) \times 10^5$Pa. The middle, ring and little fingers are coupled to cope with the small number of actuators, limiting the available force on these fingers, the hand dexterity and, due to the transmission mechanism, limiting the ability to conform in some grasps.

Keywords: robotic, hand, robust, compliant, conformable

1. Introduction

In the last decades service and social robots have achieved a remarkable level of maturity. However, within this field, the results regarding grasping and manipulation still remain limited in some aspects. Particularly, while the description of the environments where such applications occur has a limited precision and thus the hand has to be able to cope with errors in the objects position, shape and orientation, in those applications an unexpected collision is likely to occur and therefore the hand must be able to sustain impacts in that case.

To address grasping and manipulation requirements in these cases two different types of systems appear.

The first type is constituted by more complex systems as in [7], which implement complex actuation schemes as, for the referred case, the antagonistic drive train with a variable stiffness actuation mechanism which provides protection to the motors under collision and proprioception on each tendon tension. These actuation schemes, combined with a high number of actuators, enable the independent actuation of most of the degrees of freedom (DoF) of the hand, achieving remarkable robustness and very high levels of dexterity. However, these systems require the use of the forearm to place the actuators and thus result in hands that are not adaptable into different arms and which are very expensive, being almost exclusive to the centers where they are developed. Futhermore, the operation of these hands requires complex control schemes that are particularly sensible to errors in the representation of the surroundings and thus more prone to failure in social environments.

The second type is constituted by the simpler systems as in [10], which use few actuators in underactuation schemes, where one motor is made to drive several serial joints. This scheme enables the fingers to enclose around and conform to the object and thus they enable to cope with the errors in the object location, size and orientation. Although the underactuation scheme provides some protection, these systems robustness and compliance can be improved by including serial elastic actuation mechanisms, as in [11], providing protection for the robot, its workpiece and the surroundings and, as before, also enable to determine the tension of the tendons. As this type of systems use underactuation they require less actuators, resulting in smaller, more accessible systems that can achieve self-containment and be adaptable to other arms. However, most of these systems are focused only on simple grasps and therefore they are not dexterour nor able to execute manipulation tasks. An example of a system that, although underactuated and self-contained, is human-sized and achieves significant dexterity through the independent flexion of

the thumb, index and middle finger, is the IH2 Azzurra Series, presented in [14]. However, this hand only has 2 phalanges per finger, limiting the objects it can grasp.

Regarding kinematics design methods, these are classified as a function of their evaluation criteria into functional and mathematical kinematics design methods. The functional kinematics are based on pratical tests that are either custom or based on medical tests and grasping tasks ([7]), focusing on the accomplishment of the hand requirements. The kinematics designs based on mathematical criteria focus only on a subset of the hand parameter space or a functionality of the hand because of the intractable dimension of the whole hand parameter space.

For a robotic hand to be able to execute manipulation tasks it must be able to determine the object position in the hand through a tactile sensing scheme. For this purpose, although several different technologies exists, the specifications of each implementation as being the fabrication process, the encapsulation and even the data treatment, are seen to have the greatest influence in the final result. Furthermore, the comparison between different implementations is not always possible as these are characterized differently [16], [5].

2. Implementation

In this section each of the development stages are overviewed

2.1. Actuation

The actuation scheme is a crucial component of this hand as it defines the hand robustness, its dexterity and the achievement of a lightweight and self-contained system. As to combine all of these features an underactuation scheme was chosen that achieves dexterity by mapping the few actuators available to the DoF of the hand based on the functional regions of the hand considered on [9]. However, as the controller boards used only coped with four motors, the flexion of the middle, ring and little finger were coupled, leaving the thumb flexion/extension and adduction/abduction and the index flexion/extension actuated by one motor each. To complement, a non-linear serial elastic actuator (SEA) was implemented, adapted from [7], to improve robustness. The non-linear case was preferred over a linear SEA as it protects the motor over a wider range of tendon forces.

2.2. Kinematics

The definition of the hand kinematics is divided in kinematics design and the kinematics optimization of the fingers and thumb design, now presented.

2.2.1 Design

As each designed kinematics is greatly influenced by its purpose a new design was developed. Among the kinematics design methods available a functionality-based design method was used, similar to the implemented in [7]. This method uses the abstraction of the human hand functionalities and their conversion into technical implementations, previously performed based on the similar analysis of [7] and [9], to define the parameters to vary within the hand. To evaluate each set of parameters the cardboard prototype which implemented such set, as in [7] and [9], was subjected to common grasping tests and to a simplified version of the Kapandji test defined in [8]. The following list briefly describes each parameter varied and their effects of the hand performance.

- Orientation of the thumb base towards the fingers - This angle of the base joint of the thumb (TMC) defines the finger to which the thumb points to when stretched out and in front of the palm. It is defined pointing to the little finger as otherwise the thumb tip would not be able to reach the base of this finger.

- Intersection of the axis of the thumb base with the palm surface - If the first axis of the TMC intersects the palm at the base of a finger the thumb can only reach the base of that finger. This angle was set for the intersection to occur closer to the center of the palm, enabling the palm to reach the base of all fingers.

- Inclination of the medial (MP) and distal (IP) joints of the thumb - Inclination angles at the joints cause them to be straight at the stretched out position but to move the phalanges located distally out of the sagittal plane of the thumb during its flexion. These angles were defined to reorient the thumb towards the ring and middle finger and its pads towards the palm, to improve opposition and to greatly enhance the grasping performance of smaller objects.

- Twist of the IP joint of the thumb - The twist angle causes the reorientation of the thumb distal phalanx pad, even in stretched out position. This angle is set such that the thumb distal pad is reoriented towards the center of the palm, greatly enhancing the grasp of objects with large diameters.

- Angle of the little finger base joint - As the hematometacarpal joint of the little finger could not be implemented a fixed angle was set

at the base of this finger to turn it inwards towards the center of the palm, even in stretched-out position. This angle was maximized while avoiding an overlap with the ring finger.

- Inclination angles at the medial (PIP) and distal joints (DIP) of the little and ring finger - As with the thumb, these angles move the fingers phalanges out of the sagittal plane during flexion. These angle are maximized while avoiding overlap, turning the fingers towards the center of the palm to improve the opposition to the thumb and to avoid the achievement of lateral contacts with objects.

2.2.2 Optimization

With the kinematics skeleton of the hand defined, an optimization process was used to define the radius and stiffness of the fingers and thumb joints in order to improve the hand stability without affecting the hand functionalities. Following the method for a three phalanx underactuated finger with elastic joints of [1], the forces exerted by each phalanx at the contact points are calculated as a function of the joints radius and stiffness. To analyse each set of joint stiffness and radius, three different cases are considered after verifying that the force exerted by the distal phalanx is always positive:

- All the phalanges contact the object;
- Only the proximal and distal phalanges contact the object;
- Only the medial and distal phalanges contact the object.

The case where only the distal phalanx contacts the object is a composition of the last two and is very rare, thus it is not explicitly considered. The analysis criteria for the finger stability are the force positiveness criteria, which states that the a contact configuration is only stable if the contact forces exerted by the phalanges are positive or zero depending on whether the phalanx achieves contact or not, respectively, and the force uniformity criteria, which states that a finger where the contact forces are more uniformly distributed is more stable. These criteria are evaluated by the following functions:

$$\begin{aligned} \chi &= \frac{\int_W \delta_j(\boldsymbol{k}, \boldsymbol{\Delta\theta}) d\boldsymbol{k} d\boldsymbol{\theta})}{\int_W d\boldsymbol{k} d\boldsymbol{\theta}} \\ I &= \frac{\int_W \frac{\sum_{i=1}^{n} f_i}{max_i(f_i)} \delta_j(\boldsymbol{k}, \boldsymbol{\Delta\theta}) d\boldsymbol{k} d\boldsymbol{\theta})}{\int_W d\boldsymbol{k} d\boldsymbol{\theta}} \end{aligned} \quad (1)$$

where k_i is the contact point on the i^{th} phalanx and $\Delta\theta_i$ is the angular displacement of the i^{th} joint. W refers to the full workspace of the finger limited by $\Delta\theta_i \in [\Delta\theta_{0i}; \frac{\pi}{2}]$ and $k_i \in [0; l_i]$, being l_i the length of the i^{th} phalanx, and $\delta(\boldsymbol{k}, \boldsymbol{\Delta\theta})$ is a piecewise function that is different for the different grasping cases described and that is 1 whenever all the condition for each grasping case is satisfied and 0 otherwise. The term $max_i(f_i)$ refers to the highest value among the components of $\boldsymbol{f}$ in each configuration.

The joint radius and stiffness were then varied and, for each of these sets both evaluation criteria were determined for each of the three contact configurations. The ratio between joint stiffness of a joint and the stiffness of the joint located proximally was limited to the range 0.4 to 0.6, to maintain a natural finger behaviour. To analyse the data each the stability criteria was normalized within the same run and the average and mean deviation within the three contact cases of each variable set was calculated. The most stable configurations, i.e. the cases with higher normalized averages and smaller normalized mean deviations, are presented in table 1. Among those, the configuration chosen was the 3^{rd} as, since the maximum joint stiffness is defined, a greater ratio between joint stiffness result in weaker base joints and it may cause the finger to bend significantly under its own weight, which may affect the system performance. The configuration chosen for this finger, the index, is also seen to be amongst the most stable for the remaining fingers and the thumb and thus it is implemented in all of them.

2.3. Design of the Hand

The design of the hand addresses the implementation and integration of all features and mechanism into a single system. The fingers were developed first followed by the palm and the skin layer.

2.3.1 Fingers

As the joints stiffness and moment arms are the same for all fingers and the thumb, these were all developed from a single general model and were adapted afterwards. Within this model the elastic elements of the joints were defined first, followed by the tendon routing and the finger structure.

Regarding the joints elastic elements, several different prototypes were made using springs or rubber beam joints (as in [10]). For each of those prototypes a test unit was built and they were compared base on their ability to flex and extend properly and on the functionalities abstracted from a previous analysis to the human hand. Among prototypes with the rubber beam connecting the phalanges a bending element of smaller length was seen to provide the desired stiffness with smaller thickness and to limit the excessive and unnatural lateral motion of the joint. When comparing the rubber beam joint

r_2/r_1	r_3/r_2	k_{max}(Nm)	k_{ratio}	$\bar{F}_{positiv.}$	$MD(F_{positiv.})$	$\bar{F}_{uni.}$	$MD(F_{uni.})$
0.60	0.65	0.1	2.22	0.877	0.037	0.881	0.034
0.60	0.65	0.1	2.00	0.864	0.037	0.866	0.033
0.60	0.65	0.1	1.82	0.851	0.036	0.850	0.033
0.55	0.65	0.1	2.22	0.900	0.040	0.901	0.039
0.55	0.65	0.1	2.00	0.886	0.040	0.884	0.038

Table 1: Normalized results averaged over the three grasping cases and the corresponding mean deviation for both evaluation criteria of the optimization process. Only the five more stable configurations are presented. r_1, r_2 and r_3 are the radius or moment arms of the base, middle and distal joints, respectively. k_{max} is the stiffness of the stiffer joint, the distal, and k_{ration} the ratio between joint stiffness.

design to the design using springs as the elastic element it was seen that to achieve similar functionalities in the latter, as being the ability to luxate and provide robustness against lateral impacts, an implementation with more tendons would have to be performed and a more complex serial elastic actuation mechanism would have to be implemented and thus the joint design with the rubber beam element was chosen (figure 1). However, as several joints of this type in series result in a finger with excessive lateral motion the base joint of the fingers was implemented using springs, as seen in figure 1, and, as the base joint of the thumb has 2 DoF, a base joint without any elastic element is used, relying only on the pre-tension of the closed-loop tendons used to actuated these DoF to maintain the contact between the hyperboloid surfaces (figure 1).

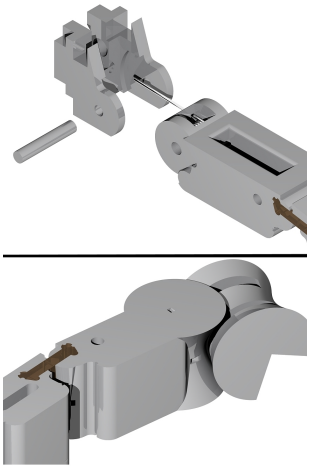

Figure 1: Base joints of the fingers (top) and the thumb (bottom).

Regarding the routing path for the tendons in the fingers two different approaches to minimize the friction were compared based on the Eytelwein equation, one where the routing angles are minimized and another where columns of other materials could be inserted in the finger to decrease friction in those sections. Given that the fingers were 3D printed in PLA, although the first case could decrease the angles up to 44% of the angles in the second case, in the latter the dyneema fibre tendons could be routed through PTFE columns, reducing the coefficient of friction by 66% in these sections when compared to friction with PLA. Besides, as the first case leads to more fragile regions within the finger structures, the second design was chosen.

The focus on the fabrication of the fingers and thumb structures was to achieve strong elements while reducing the mass, which could be achieved by using 3D printing, resulting in strong fingers with a mass of 13g each.

2.3.2 Palm

While the palm of this hand must be lightweight and approach human size it must also contain all the motors, controller boards and serial elastic actuation mechanisms. To achieve this, the motors were placed as closer as possible to the joints they actuate such that the tendon routing within the palm, which has to be cleared to achieve good force transmission, is minimum and cleared. The most complex case was for the motor driving the little, ring and middle finger, where the simpler routing was seen to be through two etched path in the posterior face of the palm, as seen in figure 2.

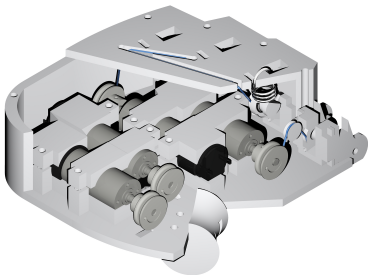

Figure 2: Inside of the palm, with tendons in blue. Besides the motors fixation, the SEA mechanism and the tendon routing in that mechanism can be seen at the base of the middle and index finger, respectively. In the posterior face of the palm the routing path for the tendons of the middle and ring fingers are shown.

As the SEA mechanism and the piece that fix-

ates the finger (figure 1, top) are the elements of the palm that are more likely to be damaged and in order to achieve a more compact implementation, these two elements are combined into a single module and this module is separated from the rest of the palm in order to ease the assembly and repair of the hand. The motors are fixated by a piece that is bolted to the palm, exerting pressure on the motors.

2.3.3 Skin

To define the skin layer of this hand the analysis presented in [3] and [15] were followed and, as a result, a soft elastomer skin with threads was chosen, similar to the implementation in [10]. Furthermore, this implementations is particularly fit to the tactile sensing scheme implemented, which is described in the following section.

2.4. Sensors

Within the sensors types reviewed in [16] and [5], the ones that are more adequate to this system are the embedded MEMS strain gauges and piezoresistors, the embedded capacitive sensors of the magnetoresistive sensors. Among those, while the sensors using MEMS have their robustness affected by the exposed fragile sensing element, the capacitive sensors require complex wiring schemes, which affect their integration in the system. Thus, a magnetoresistive tactile sensor based on spin-valves was modelled and afterwards fabricated in INESC-MN under supervision of professor Susana Freitas. To model the system the field generated by the used magnet of dimensions $1.0 \times 1.5 \times 5$mm and remanent magnetization of $1050\frac{kA}{m}$ was determined using the Colombian model of the magnetic field and the sensors position was defined such that the average field in the sensors volume varies the most between the rest and most compressed position of the skin layer, distanced by 2mm in zz, while maintaining this field within the linear range of the sensor, which is within 0 and 30 Oe. Under these conditions 4 sensors were positioned at $(\pm 0.7; \pm 2; 6)$mm from the centre of the magnet on the rest position, forming a rectangle.

To test the sensors the setup of figure 3 was used where a pad with the same material and design of the hand skin has the magnet embedded and aligns it with the sensors below and the pressure exerting tip above. The tip is then loaded with washers of known mass and the sensor output is read. The sensor is seen to present a creep behaviour related to the elastomer material used which disturbs the measures but can be solved as seen in [13] and, also, under higher loads the magnet rotates due to its small dimensions in the xx direction, disturbing the repetition of measurements.

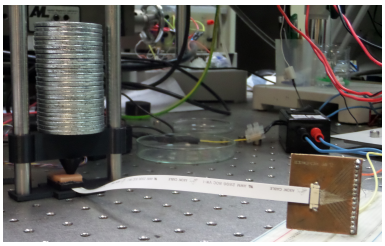

Figure 3: Experimental setup used to test the sensors.

Regarding the results, the sensors response to increasing loads is non-linear as seen in figure 4 and may be use to calibrate the sensors to measure the applied pressure. From these results the sensors resolution is seen to be under $(2.513 \pm 0.040) \times 10^4$ Pa and a force sensing range greater than $(7.123 \pm 0.016) \times 10^5$Pa since the sensor output is only seen to vary 0.021 mV under that pressure while the maximum output variation of the sensors is seen to be 0.24 mV.

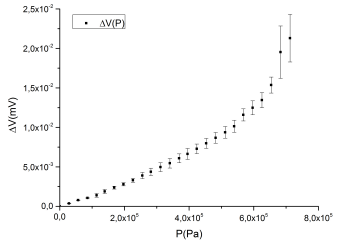

Figure 4: Output response of the sensors to the applied pressure.

Testing the sensor output repeatability under the same load 30 measurements were made and, from these results, a mean and standard deviation of

$$\begin{aligned} \bar{V} &= \frac{\sum_{i=1}^{n} x_i}{n} = 6.90\mu V \\ \sigma(V) &= \sqrt{\frac{\sum_{i=1}^{n}(x_i - \bar{x})^2}{n}} = 0.26\mu V \end{aligned} \tag{2}$$

were achieved, proving that this sensors may be used to measure the exerted pressure.

Finally, the capability to determine the contact point location is assessed by applying pressure directly above one of the corners of the magnet and comparing the response of each sensor to that of the reference position previously measured. The results obtained are presented in table 2, where the sensor 4 is the closest to the point where the pressure is exerted and the sensor 1 is the sensor that is most distant to the point where the pressure is applied. While the sensors 4 and 3 are the ones that vary the most, respectively, indicating that the force is

Measure	ΔV_{s1} (μV) ($\pm\delta_{exp}$)	ΔV_{s2} (μV) ($\pm\delta_{exp}$)	ΔV_{s3} (μV) ($\pm\delta_{exp}$)	ΔV_{s4} (μV) ($\pm\delta_{exp}$)
1	-1.340 ± 0.014	-1.520 ± 0.014	9.040 ± 0.014	11.630 ± 0.014
2	0.910 ± 0.014	-1.290 ± 0.014	2.730 ± 0.014	4.960 ± 0.014
3	1.030 ± 0.014	0.290 ± 0.014	3.980 ± 0.014	5.790 ± 0.014

Table 2: Results regarding the determination of the tactile contact point using the output tensions of all four sensors. The errors presented are experimental errors obtained through quadratic propagation.

applied near those, the variations of the sensors 1 and 2 fail to provide useful contributions, possibly due to the creep behaviour.

2.5. Software and Control

To control the motors in the hand the MC4/MCP controller boards developed for the iCub project were chosen as they are seen to provide the more compact and accessible system and to only require one more MC4 board to double the number of used motors since the MCP board can power up to 4 MC4 boards. Regarding software, the YARP and iCub repositories already provide the boards firmware and the drivers for the boards to control the motors. The robotInterface module of the iCub software repository was used to make the interface with the hardware and to configure it. This module creates the ports to address and command the motors. As the robot to which the hand will be adapted to uses the ROS platform, the software to control the motors implements a service, i.e. a client-server scheme, where the server is implemented in YARP and is used to decode the messages from the user and to feed the low-level commands to the ports created by the robotInterface and the client is implemented in ROS and is operated by the user that can place independent requests for each motor, being able to either send lower level commands as a specific positions achieved with specific velocities and acceleration or more high-level commands as simply requesting the fingers and the thumb to flex completely. The ROS node then encodes the users request into a custom type message, sends it to the YARP module which decodes the message into motor commands, sends it to the boards and then replies to the ROS node with encoders readings.

To control the motors a PID controller embedded in the boards firmware was used and its parameters were tuned using the fingersTuner module of the iCub software, described in [12]. The obtained tuned parameters are presented in 3.

Motor (Controlled DoF)	K_P	K_I
1 (Thumb abd.)	-5.33	-121
2 (Thumb flexion)	-6.70	-199
3 (Index finger flexion)	-9.80	-329
4 (Middle, ring, little finger flexion)	-5.27	-139

Table 3: Results for the tuning of the PI controller parameters.

3. Results

The characterization of the hand was performed in three stages. In the first stage a general characterization of the aesthetics and the parameters that enable its adaptation into other arms as the mass are addressed. In the second stage the hand operation and grasping performance are evaluated. In the third stage the hand robustness is assessed.

3.1. General characterization

While the hand aesthetics are relevant to the use in applications with human interactions the hand is also intended to be adaptable into different arms.

Regarding the aesthetics, the hand is seen to be human sized (figure 5) and, as the mechanical friction in the joints is reduced or non-existent the fingers motion is fluid. With the focus on hand performance the aesthetics were not fully addressed resulting in an unappealing aspect of the hand.

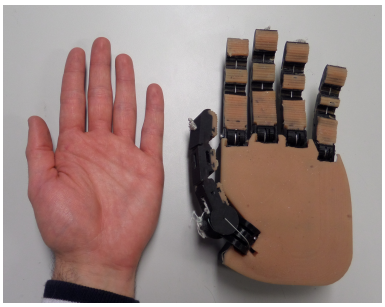

Figure 5: Comparison of the size of the human hand and the final prototype

Regarding the adaptation into other arms the hand is self-contained apart from the CAN-USB converter used. To achieve self-containment the hand height was set at 37.5mm, which, compared to the 45mm of the IH2 Azzurra hand ([14]) or the 63mm of the Meka H2 hand ([11]), is seen to be compact. Furthermore, it has a mass of 0,57kg without the converter, which has a mass of 0,07kg, and thus it is among the lightest existing systems, with OpenHand Model T ([10]) having a mass of 0,49kg and the IH2 Azzurra Hand ([14]) having a mass of 0,64kg.

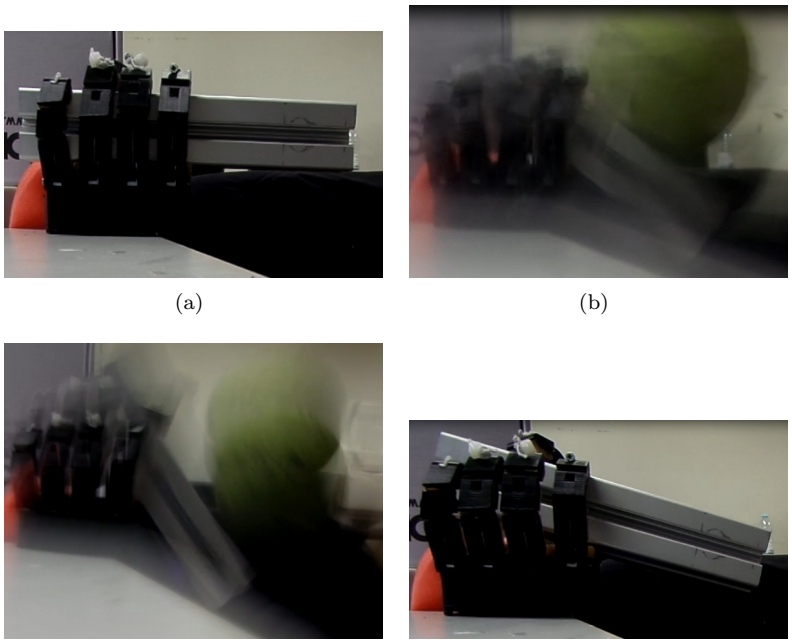

(a) (b)

(c) (d)

Figure 6: Robustness test of the last prototype

3.2. Grasping performance

To assess the grasping performance of the hand the grasps in the Feix [6] and Cutkosky [4] taxonomies were attempted, as they have already been previously used to evaluate dexterous hands as the Awiwi hand ([7]) or the Robonaut 2 hand ([2]).

The accomplished grasps are presented in figures 7 and 8 for the Cutkosky and Feix taxonomies, respectively. The hand is seen to accomplish 41 of the 49 grasps in those taxonomies, including most of the precision grasps, and thus the hand is seen to achieve a significant level of dexterity.

During this evaluation two types of impairments were noted in the hand, which are now described.

The first type of limitations are related to the iterative hand development method and include three different flaws. The first is that the little, ring and middle fingers, which are coupled, are seen to stop as soon as one of them conforms with the object, impairing the contact achieved by the other two fingers. This occurs because the fingers are all directly connected to the same motor, which is also seen to affect the contact forces exerted by these fingers, requiring an improved force transmission mechanism. The second flaw is that the fingers are unable to contact the palm because the base and middle joint are limited to 90^o flexion, requiring the fingers design to be changed. The third flaw is that the motors in the palm and the tendons in the fingertips are not properly fixed, being able to move and requiring regular recalibration due to the deformation of the 3D printed pieces.

The second type of limitations are related to the design choices performed throughout the design process and, specifically, to the disabled DoF of the hand, as the little finger hematometacarpal joint and the sideways motion of the fingers base joints, and the couplings performed due to the small number of motors used, as the coupling of the middle, ring and little finger. These limitations are mostly seen in grasps the first grasps of columns 2-3, 2-4 and 2-5 of the precision grasps with pad contact of the Feix taxonomy, which could not be performed by this hand.

3.3. Robustness

The term robustness means, in this context, that, under collision, the hand not only maintains its integrity but also avoids damaging the surroundings and its workpiece. In this context, the hand reaction to collisions in the posterior and anterior surfaces of the fingers were assessed and also its maximum payload.

Regarding collisions with the posterior face of the fingers, the fingers are seen to easily flex and, as the tendon is not extended in the process, no damage is likely to occur, whether to the fingers or the surroundings.

Regarding collision with the anterior face of the fingers, although the fingers are made compliant by the SEA mechanism used, this mechanism can only protect to a certain point and thus, under high impacts the motor may be damaged. To asses the protection provided by this mechanism and the protection offered to the hand workpiece a test was

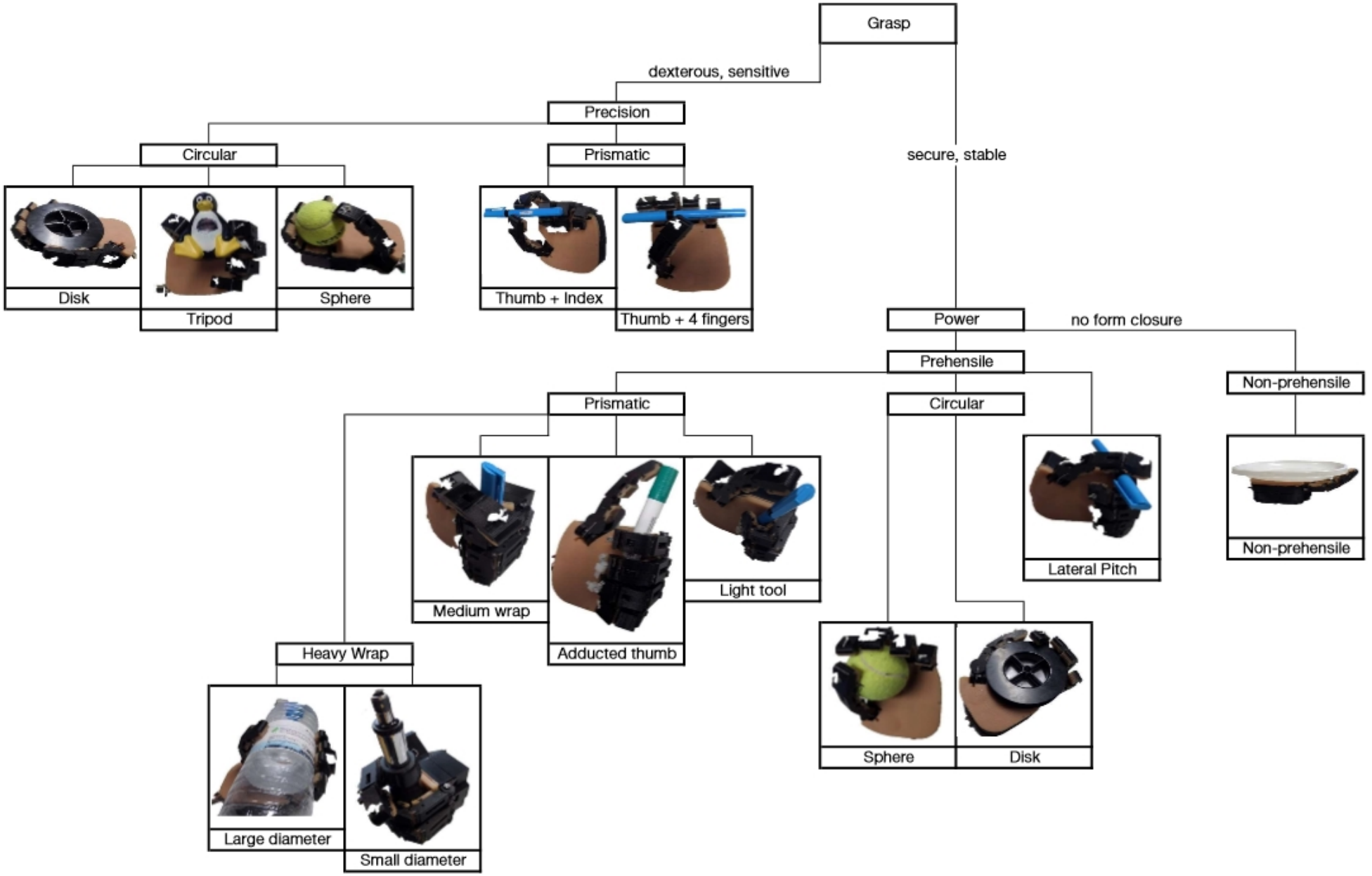

Figure 7: Grasps of the Cutkosky taxonomy that were successfully accomplished by the developed hand.

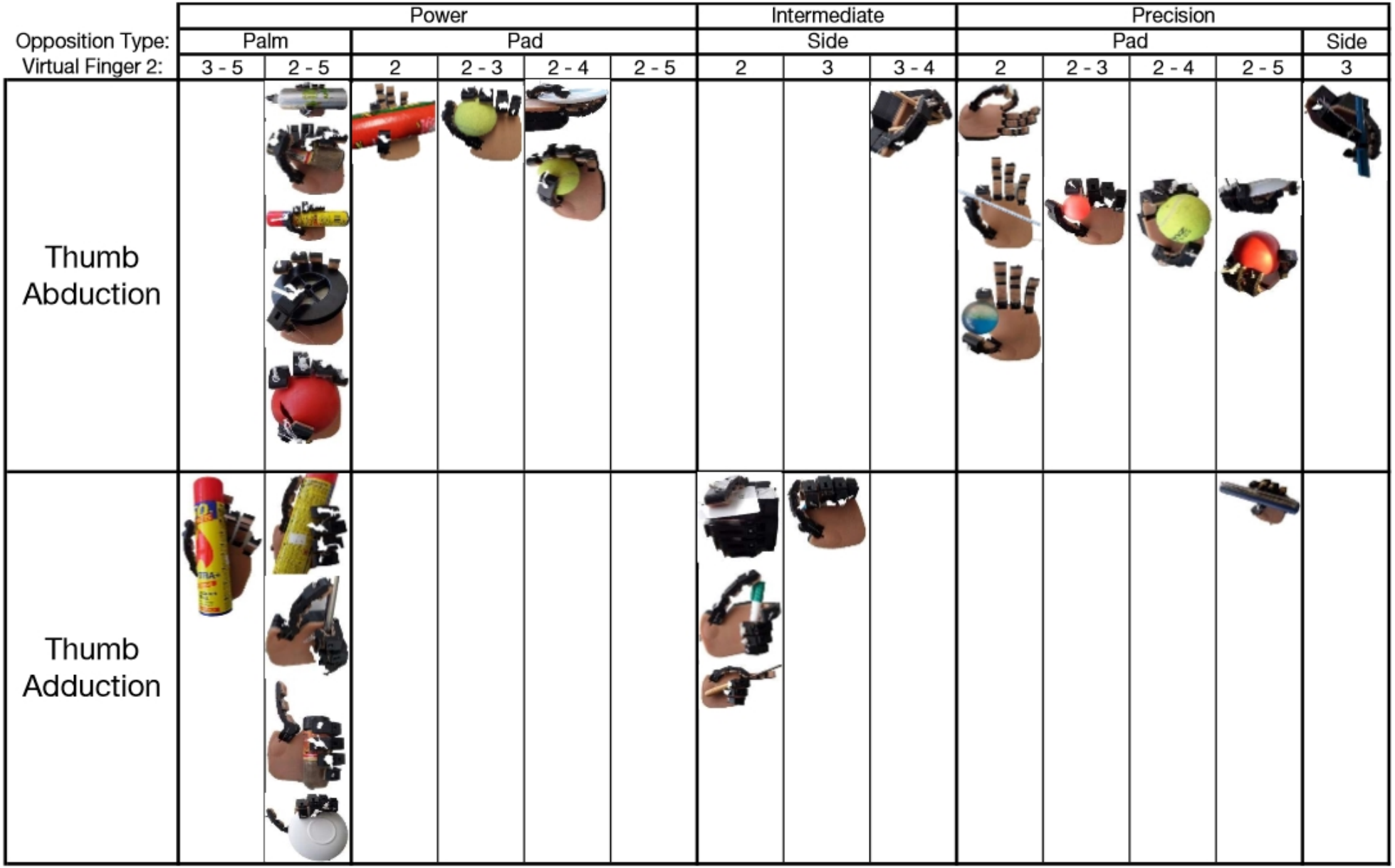

Figure 8: Grasps of the Feix taxonomy that were successfully accomplished by the developed hand.

performed where a ball with 300g mass is dropped from an height of 1,8m to a column of 345g mass that is being grabbed by the hand. The collision is depicted in figure 6 where the hand is able to sustain the impact without being damaged and still keep the object grasped.

The maximum payload of the hand was evaluated to be 2kg for an object completely enclosed by the fingers and 4.5kg for a load placed on a bag that is sustained by the fingers.

4. Conclusions

The developed hand is seen to be human-sized, self-contained and, with a reduced mass of 0,57kg and a height of 37,5mm, the hand presents specifications that are in line with those presented by the most advanced similar systems. Besides, the hand can accomplish 41 of 49 grasps in the Feix and Cutkosky taxonomy, achieving a significant level of dexterity that, although inferior to those of the Awiwi hand and the Robonaut 2 hand, this difference is mainly due to the very limited number of motors this hand is required to have and not due to the kinematics design. This hand is seen to be robust, assuring not only its integrity but also the integrity of its workpiece when a large ball is dropped on a column grasped by the hand, which is still grasped after the collision. The hand presents a maximum payload of 4.5kg which is the highest reported among similar systems. A magnetoresistive tactile sensor was developed that presents a non-linear response, a resolution under $(2.513 \pm 0.040) \times 10^4$ Pa and a force sensing range greater than $(7.123 \pm 0.016) \times 10^5$Pa. Despite the development of this sensors, its data acquisition electronics and its data treatment were not addressed and, as such, the hand was not provided with manipulation capabilities. Also, such manipulation capabilities are greatly impaired by the coupling of the middle finger to the ring and little fingers. The hand is seen to require further development to achieve a stable and completely autonomous operation.

References

[1] L. Birglen, C. Gosselin, and T. Laliberté. *Underactuated Robotic Hands*. Springer Tracts in Advanced Robotics. Springer, 2008.

[2] L. Bridgwater, C. Ihrke, M. Diftler, M. Abdallah, N. Radford, J. Rogers, S. Yayathi, R. Askew, and D. Linn. The robonaut 2 hand - designed to do work with tools. In *Robotics and Automation (ICRA), 2012 IEEE International Conference on*, pages 3425–3430, May 2012.

[3] M. Cutkosky, J. Jourdain, and P. Wright. Skin materials for robotic fingers. In *Robotics and Automation. Proceedings. 1987 IEEE International Conference on*, volume 4, pages 1649–1654, Mar 1987.

[4] M. R. Cutkosky. On grasp choice, grasp models, and the design of hands for manufacturing tasks. *Robotics and Automation, IEEE Transactions on*, 5(3):269–279, 1989.

[5] M. Fässler. Force sensing technologies. 2010.

[6] T. Feix, H. bodo Schmiedmayer, J. Romero, and D. Kragi. A comprehensive grasp taxonomy. In *In robotics, science and systems conference: workshop on understanding the human hand for advancing robotic manipulation.*, 2009.

[7] M. Grebenstein. *Approaching human performance: The functionality driven Awiwi robot hand*. PhD thesis, ETH Zurich, 2012.

[8] A. Kapandji. Cotation clinique de l'opposition et de la contre-opposition du pouce. *Annales de Chirurgie de la Main*, 5(1):67 – 73, 1986.

[9] I. Kapandji. *The Physiology of the Joints: Upper limb*. Physiology of the Joints. Churchill Livingstone, 1982.

[10] R. R. Ma, L. U. Odhner, and A. M. Dollar. A modular, open-source 3d printed underactuated hand. In *Robotics and Automation (ICRA), 2013 IEEE International Conference on*, pages 2737–2743. IEEE, 2013.

[11] Meka Robotics. Meka h2 compliant hand technical specifications.

[12] U. Pattacini. Online tuning of pid controllers. Technical report, Istituto Italiano di Tecnologia, iCub Facility, 2013. Avilable at: https://files.zenhub.io/54b65e1aa249c8781446c7a6.

[13] K. L. Phan. Methods to correct for creep in elastomer-based sensors. In *Sensors, 2008 IEEE*, pages 1119–1122, Oct 2008.

[14] Prensilia s.r.l. Prensilia s.r.l. ih2 azzurra series data sheet.

[15] K. Shimoga and A. Goldenberg. Soft materials for robotic fingers. In *Robotics and Automation, 1992. Proceedings., 1992 IEEE International Conference on*, pages 1300–1305 vol.2, May 1992.

[16] H. Yousef, M. Boukallel, and K. Althoefer. Tactile sensing for dexterous in-hand manipulation in roboticsa review. *Sensors and Actuators A: Physical*, 167(2):171 – 187, 2011. ¡ce:title¿Solid-State Sensors, Actuators and Microsystems Workshop¡/ce:title¿.